Pre-conditioning modifies the TME to enhance solid tumor CAR T cell efficacy and endogenous protective immunity

John P. Murad,[1] Dileshni Tilakawardane,[1] Anthony K. Park,[1,2] Lupita S. Lopez,[1,2] Cari A. Young,[1,2] Jackson Gibson,[1] Yukiko Yamaguchi,[1] Hee Jun Lee,[1] Kelly T. Kennewick,[1] Brenna J. Gittins,[1] Wen-Chung Chang,[1] Chau P. Tran,[7] Catalina Martinez,[5] Anna M. Wu,[4] Robert E. Reiter,[7] Tanya B. Dorff,[6] Stephen J. Forman,[1,3] and Saul J. Priceman[1,3]

[1]Department of Hematology and Hematopoietic Cell Transplantation, City of Hope, Duarte, CA 91010, USA; [2]Irell and Manella Graduate School of Biological Sciences, City of Hope, Duarte, CA 91010, USA; [3]Department of Immuno-Oncology, Beckman Research Institute of City of Hope, Duarte, CA 91010, USA; [4]Department of Molecular Imaging and Therapy, City of Hope, Duarte, CA 91010, USA; [5]Department of Clinical and Translational Project Development, City of Hope, Duarte, CA 91010, USA; [6]Department of Medical Oncology and Therapeutics Research, City of Hope, Duarte, CA 91010, USA; [7]Department of Urology, University of California, Los Angeles, Los Angeles, CA 90095, USA

Chimeric antigen receptor (CAR) T cell therapy has led to impressive clinical responses in patients with hematological malignancies; however, its effectiveness in patients with solid tumors has been limited. While CAR T cells for the treatment of advanced prostate and pancreas cancer, including those targeting prostate stem cell antigen (PSCA), are being clinically evaluated and are anticipated to show bioactivity, their safety and the impact of the immunosuppressive tumor microenvironment (TME) have not been faithfully explored preclinically. Using a novel human PSCA knockin (hPSCA-KI) immunocompetent mouse model, we evaluated the safety and therapeutic efficacy of PSCA-CAR T cells. We demonstrated that cyclophosphamide (Cy) pre-conditioning significantly modified the immunosuppressive TME and was required to uncover the efficacy of PSCA-CAR T cells in metastatic prostate and pancreas cancer models, with no observed toxicities in normal tissues with endogenous expression of PSCA. This combination dampened the immunosuppressive TME, generated pro-inflammatory myeloid and T cell signatures in tumors, and enhanced the recruitment of antigen-presenting cells, as well as endogenous and adoptively transferred T cells, resulting in long-term anti-tumor immunity.

INTRODUCTION

Despite clinical successes of chimeric antigen receptor (CAR)-engineered T cell therapies in hematological malignancies, effective CAR T cell therapies in solid tumors have been limited.[1–3] Immunotherapies for solid tumors are restricted by the tumor microenvironment (TME), which includes, among others, tumor-associated macrophages (TAMs), myeloid-derived suppressor cells (MDSCs), and regulatory T cells (Tregs), all of which suppress endogenous immunity, as well as adoptively transferred T cell trafficking, persistence, and anti-tumor activity.[1,4,5] Alleviating immunosuppression in solid tumors and improving CAR T cell-mediated anti-tumor activity is an active, but still very early, area of research and includes targeting immune checkpoint (e.g., PD-1 and CTLA-4) and/or other immunomodulatory pathways. Pre-conditioning chemotherapy has been widely employed in combination with CAR T cell therapy, particularly in the setting of hematological malignancies. This approach has classically been described as "space-making" lymphodepletion to enhance homeostatic cytokine production for improved adoptively transferred T cell engraftment.[6,7] However, the totality of benefits and underlying mechanisms of action of this approach for solid tumors is still controversial.[8] Studies that more faithfully assess the safety and efficacy of this approach in the context of solid tumor CAR T cell therapies will require more comprehensive preclinical models.[9]

Our group has recently initiated a phase 1 clinical trial to evaluate the safety, feasibility and biological activity of prostate stem cell antigen (PSCA)-directed CAR T cells in patients with metastatic castration-resistant prostate cancer (mCRPC), based on extensive preclinical optimization using human xenograft models.[10] As with most solid tumor-associated antigens (TAAs, e.g., HER2, CEA, PSMA, and mesothelin), PSCA expression in normal tissues, including the stomach, bladder, pancreas, and prostate, may pose safety concerns or limit the therapeutic benefits of CAR T cells.[11,12] While studies using immunocompromised mice allow for evaluating the activity of CAR T cells in vivo for clinical translation, these immunocompromised mice typically lack a physiologically normal tissue expression of TAAs, which precludes assessment of potential "on-target, off-tumor" toxicities. Additionally, they fail to capture the complexity of the local TME and the impact of immunotherapy on systemic immunity. These components may contribute to some of the key

discrepancies in clinical CAR T cell responses observed in hematological malignancies and solid tumors.[13,14]

In the current study, we developed an immunocompetent mouse model that allows simultaneous assessment of safety and anti-tumor efficacy of PSCA-CAR T cells. Our knockin mouse system allowed for expression of human PSCA (hPSCA) under the control of the mouse PSCA promoter in normal tissues. This model enabled us to evaluate PSCA-CAR T cell therapy in the context of a host with an intact immune system and the ability to comprehensively interrogate mechanisms underlying response and/or resistance to CAR T cell therapy. We found that PSCA-CAR T cells were ineffective in eliciting *in vivo* anti-tumor responses unless given after lymphodepleting pre-conditioning with cyclophosphamide (Cy). Mechanistically, we showed that the benefits of Cy pre-conditioning were attributed to early changes in the TME, including pro-inflammatory myeloid cell modifications, improved antigen presentation pathways, and profound tumor infiltration of both endogenous and adoptively transferred T cells. Combining Cy pre-conditioning with PSCA-CAR T cells resulted in durable curative responses and subsequent protective immunity against tumor rechallenge. Importantly, potent PSCA-CAR T cell anti-tumor responses were not associated with adverse effects on normal tissues expressing PSCA or other overt off-tumor toxicities. These findings inform ongoing clinical trials and further provide a preclinical platform for rational combination designs to maximize safety and efficacy of immunotherapies for PSCA⁺ solid tumors.

RESULTS

Murine PSCA-CAR T cells demonstrate selective *in vitro* activation against PSCA⁺ murine tumor cells

We generated a fully murine PSCA-CAR retroviral construct (PSCA-mCAR) targeting hPSCA. Importantly, the hPSCA targeting scFv used (clone 1G8) is the same clone that was subsequently humanized to generate our current phase 1 clinical trial (NCT03873805) lead therapeutic candidate (Figure 1A).[10] PSCA-mCAR retrovirus yielded efficient transduction of murine splenic CD4/CD8 T cells (Figure 1B, top) as determined by cell surface expression of mCD19t, and by CAR scFv expression as assessed by protein L staining, on total CD3⁺ T cells (Figure 1B, bottom). Further phenotypic analysis of both Mock and PSCA-mCAR T cells shows CD44^hi, CD62L^hi, and CCR7^hi expression, corresponding to a central memory T cell (Tcm) state (Figure S1).[15] *In vitro* antigen-specific activity of PSCA-mCAR T cells was assessed by co-culture of wild-type RM9 (hPSCA⁻) or RM9-hPSCA tumor cells with freshly transduced PSCA-mCAR T cells, resulting in antigen-dependent secretion of murine interferon-γ (IFN-γ) and interleukin-2 (IL-2) cytokines (Figures 1C and 1D). PSCA-mCAR T cells also showed antigen-dependent activation and exhaustion markers murine 4-1BB and PD-1, respectively, at varying effector:tumor (E:T) ratios (Figure 1E). RM9-hPSCA tumor cells exhibited CAR T cell-dependent increases in PD-L1 *in vitro*, presumably in response to IFN-γ secretion by activated CAR T cells (Figure 1F). CAR T cell-mediated killing of RM9-hPSCA tumor cells increased from 24 h and 72 h (Figure 1G). Additionally, PSCA-mCAR T cells also expanded following 72 h co-culture (Figure 1H).

These data show that our fully murine PSCA-CAR T cells exhibit strong antigen-specific activity against murine tumors expressing hPSCA.

PSCA-mCAR T cells lack *in vivo* therapeutic efficacy in immunocompetent mice

To investigate the safety and efficacy of PSCA-CAR T cells in an immunocompetent system, we utilized a recently developed hPSCA knockin (hPSCA-KI) mouse model.[16] We used heterozygous mice (hPSCA-KI^het; Figure S2A), to allow for engraftment of RM9-hPSCA tumor cells that may express both endogenous murine and engineered hPSCA. Using flow cytometry, immunohistochemistry (IHC), and RNAScope analyses of normal and tumor tissues, we observed low to moderate levels expression of hPSCA, relative to RM9-hPSCA tumors, in normal prostate epithelia, bladder, and stomach, mimicking expression patterns observed in humans (Figures S2B–S2D).[16,17]

Safety and efficacy of PSCA-CAR T cells were assessed in hPSCA-KI mice bearing subcutaneous (s.c.) RM9-hPSCA tumors treated with either Mock (untransduced) or PSCA-mCAR T cells by intravenous (i.v.) delivery. In contrast to the potent activity seen in previously published human xenograft models,[10] we observed minimal anti-tumor responses in hPSCA-KI mice treated with PSCA-mCAR T cells (Figure S3A). Encouragingly, no overt toxicities including visual weight loss or gross anatomical defects to normal organs upon euthanasia were observed in these mice. Interestingly, lymphocyte-deficient RAG2⁻/⁻ mice bearing RM9-hPSCA tumors treated singularly with PSCA-mCAR T cells demonstrated curative responses in 33% of treated mice (Figure S3B), highlighting the therapeutic potential of these CAR T cells in immunocompromised mice and also suggesting that in immunocompetent mice, the intact endogenous immune system is likely contributing to a suppressive TME, which resulted in limited efficacy of PSCA-mCAR T cells alone.

In vivo efficacy of PSCA-mCAR T cells in immunocompetent mice requires Cy preconditioning

Given the observed efficacy of PSCA-mCAR T cells in lymphocyte-deficient RAG2⁻/⁻ mice but not in immunocompetent hPSCA-KI mice (Figure S3), we assessed whether lymphodepleting pre-conditioning could improve the therapeutic impact of PSCA-mCAR T cells in this model. An *in vivo* Cy dose titration using a single intraperitoneal (i.p.) dose of Cy (50, 100, or 200 mg/kg) in hPSCA-KI mice resulted in a dose-dependent peripheral lymphodepletion in each immune subset evaluated, with a maximal lymphodepletion achieved 4 days following Cy treatment (Figure S4A–S4E). The anti-tumor activity of Cy alone was then examined in intratibial (i.ti.) tumor-bearing hPSCA-KI mice. From these studies we determined that in this model a single i.p. 100 mg/kg dose of Cy could provide adequate peripheral lymphodepletion, with minimal anti-tumor activity and an absence of survival benefit (Figure S4F).

We next evaluated the impact of 100 mg/kg Cy pre-conditioning in combination with PSCA-mCAR T cell therapy *in vivo*. PSCA-mCAR T cells or Cy treatment alone showed essentially no or only transient
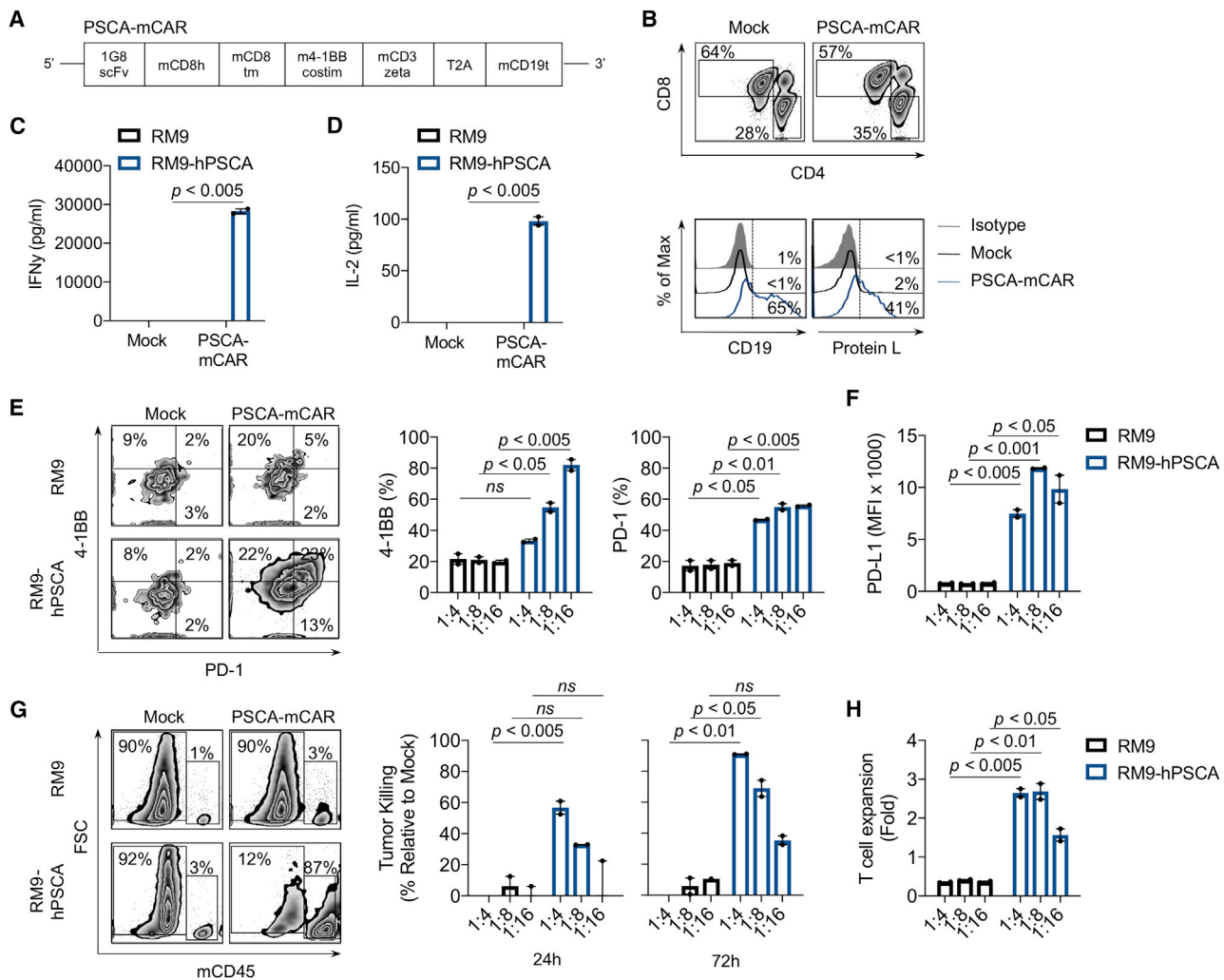
Figure 1. Characterization of PSCA-mCAR T cell transduction and activity *in vitro*

(A) Diagram of the fully murine retroviral expression cassette with PSCA-mCAR T cell containing murine scFv (1G8 clone) targeting human PSCA (hPSCA). A truncated non-signaling murine CD19 (CD19t), separated from the CAR sequence, was expressed for identifying transduced T cells. (B) Flow cytometry detection of CAR transduction measured by CD19t expression and CAR (scFv) surface detection by Protein L staining on Mock (untransduced) and PSCA-mCAR T cells (bottom) and CD4 and CD8 expression (top). (C and D) IFN-γ (C) and IL-2 (D) secretion, as measured by ELISA, by Mock and PSCA-mCAR T cells after 24 h co-culture with antigen-negative RM9 and antigen-positive RM9-hPSCA. For ELISA, N ≥ 2 replicates per group. (E) Representative flow cytometry plots depicting %4-1BB and %PD-1 induction on Mock or PSCA-mCAR after 72 h co-culture with RM9 or RM9-hPSCA (left) and quantification of %4-1BB and %PD-1 expression at indicated E:T ratios (right). (F) Quantification of mean fluorescent intensity (MFI) of PD-L1 expression on indicated cancer cells after 72 h co-culture with Mock or PSCA-mCAR T cells. (G) Representative 72 h flow cytometry plots of co-cultures of RM9 or RM9-hPSCA with Mock or PSCA-mCAR T cells showing DAPI negative, CD45-negative (remaining viable tumor cells) or CD45-positive (T cell expansion; left), and quantification of killing at 24 and 72 h post co-culture at indicated E:T ratios (right). (H) Quantification of fold expansion of Mock or PSCA-mCAR T cells after 72 h co-culture with RM9 or RM9-hPSCA. For co-culture flow cytometry data, N ≥ 3 replicates per group. All data are representative of two independent experiments. p values were determined using unpaired Student's t test.

anti-tumor activity against RM9-hPSCA tumors, respectively, and neither provided durable survival benefits (Figure 2A). However, the combination of PSCA-mCAR T cells with Cy pre-conditioning elicited robust anti-tumor activity, improved overall survival, and complete responses (CRs) in over 40% of mice (Figures 2B and 2C). This therapeutic activity was PSCA target specific, as the combination of either Mock (untransduced) T cells or T cells transduced with a functional non-

PSCA targeting CAR (NT-mCAR) with Cy pre-conditioning showed no improvements in anti-tumor activity (Figure S5). These data strongly suggest that pre-conditioning in this model is required to unleash the therapeutic potential of PSCA-mCAR T cells. Importantly, no overt toxicities or gross changes in cellular architecture to hPSCA expressing normal tissues (prostate, bladder, stomach) were observed at early and later time points post T cell treatment in any of the treated
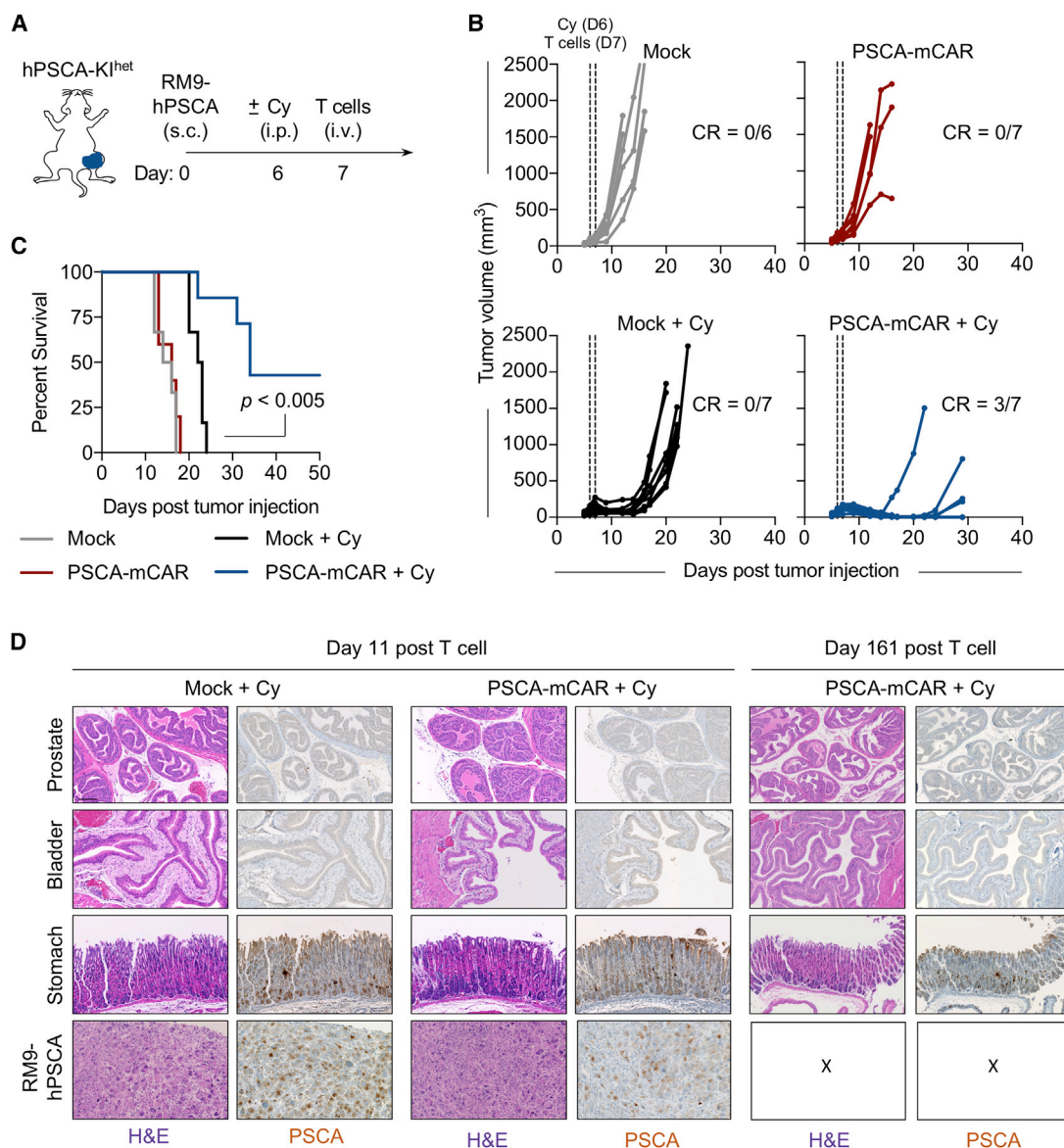
Figure 2. Anti-tumor effect of PSCA-mCAR following Cy mediated pre-conditioning and histological evaluation of normal tissue architecture and PSCA expression following treatment *in vivo*

(A) Illustration of RM9-hPSCA s.c. tumor engraftment and Cy pre-conditioning (vehicle or Cy 100 mg/kg, i.p.) 24 h prior to treatment with 5.0×10^6 T cells (Mock or PSCA-mCAR, i.v.). (B) Tumor volume (mm^3) measurements of each replicate at indicated days post tumor injection for indicated treatment with or without Cy pre-conditioning; CR, complete response. (C) Kaplan-Meier survival plot for mice in each group indicated. N ≥ 6 mice per group. p value indicates difference between Mock + Cy and PSCA-mCAR + Cy as determined by log rank (Mantel-Cox) test. (D) Representative IHC (H&E and PSCA protein staining) of indicated normal tissues from Cy pre-conditioned tumor-bearing mice at day 11 (left) or day 161 (right) post Mock or PSCA-mCAR T cells injection. All images at 20× magnification; scale bar represents 100 μm.

mice, including the combination of PSCA-mCAR T cells and Cy (Figure 2D).

Cy reverts T cell exclusion and promotes tumor infiltration of CAR T cells

We next evaluated the effects of Cy on the local TME. Tumors were initially harvested at day 3 post CAR T cell therapy and analyzed by

IHC. Interestingly, a clear T cell exclusion phenotype was observed in tumors from mice treated with Mock or PSCA-mCAR T cells alone, with T cells relegated to the normal tissue periphery and only few T cells within the tumor (Figure 3A; Figure S6). Following Cy pre-conditioning, T cells were observed at a much higher frequency within the tumor, which was greatly enhanced in combination with PSCA-mCAR T cell treatment. These data, coupled with impressive
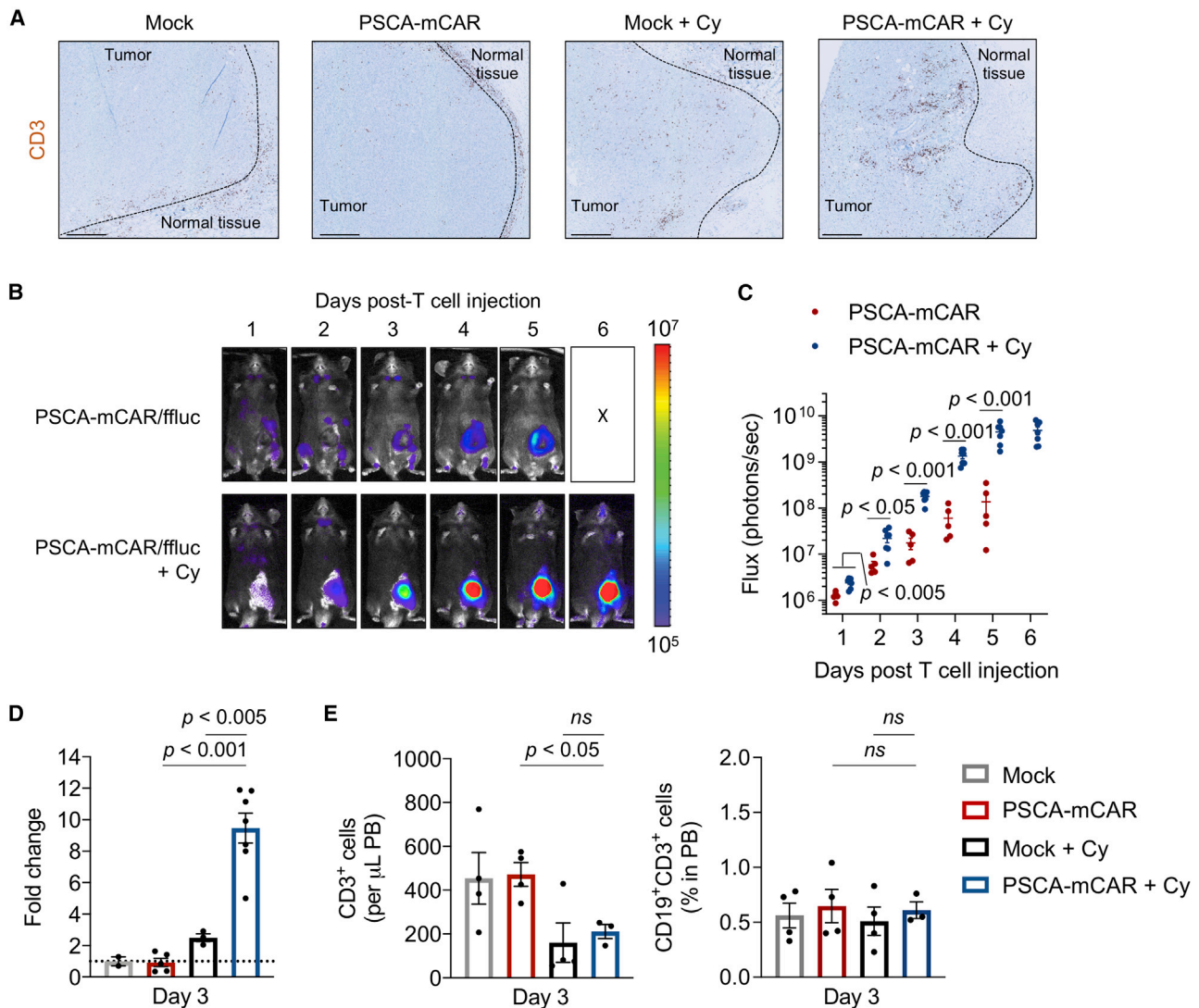
Figure 3. Cy pre-conditioning improves intra-tumoral PSCA-mCAR T cell accumulation and expansion *in vivo*

(A) IHC of CD3 T cell localization in representative RM9-hPSCA tumors harvested 3 days post T cell injection in all treatment groups. (B) Time-course bioluminescent flux imaging in RM9-hPSCA tumor-bearing mice following injection of *ffluc*-positive PSCA-mCAR T cells with or without Cy (100 mg/kg i.p.) pre-conditioning. (C) Quantification of PSCA-mCAR/ffluc T cell flux on days 1 through 6 post T cell injection with or without Cy pre-conditioning. N ≥ 5 mice per group. (D) Fold change in PSCA-mCAR/ffluc T cell flux on day 3 post T cell injection from (B) and (C). (E) Flow cytometry quantification of total CD3$^+$ T cell counts per µL PB (left) and %PSCA-mCAR (%CD19$^+$ gated on total CD3$^+$) found in PB (right) collected from mice on day 3 post T cell injection with or without Cy pre-conditioning. N ≥ 5 mice per group. IHC 5× magnification; scale bar represents 500 µm. All data are representative of two independent experiments. p values were determined using unpaired Student's t test.

in vivo anti-tumor responses with the combination (Figure 2), suggest that Cy may revert T cell exclusion within the TME.

We then quantified the kinetics of PSCA-mCAR T cell trafficking with or without Cy pre-conditioning. hPSCA-KI mice s.c. engrafted with RM9-hPSCA (non-firefly luciferase [ffluc] expressing) received Cy pre-conditioning followed 24 h later with i.v. ffluc-expressing Mock/ffluc or PSCA-mCAR/ffluc T cells. Mice were imaged daily to monitor CAR T cell biodistribution (Figure 3B). We observed significant increases of intratumoral PSCA-mCAR T cell flux in Cy pre-condi-

tioned mice as early as 24 h post T cell treatment (Figure 3C) as compared with mice treated with PSCA-mCAR T cells alone where T cell signal was predominantly confined at the tumor periphery. Interestingly, the early intratumoral accumulation of CAR T cells was observed prior to maximal Cy-mediated peripheral lymphodepletion in our model. By day 3 post CAR T cell treatment, intratumoral proliferation/expansion of CAR T cells following Cy pre-conditioning was nearly 10-fold higher than with CAR T cells alone (Figure 3D). Furthermore, analysis of peripheral blood (PB) at days 1, 3, or 10 post T cell treatment, and tumor-draining lymph nodes at 7 days
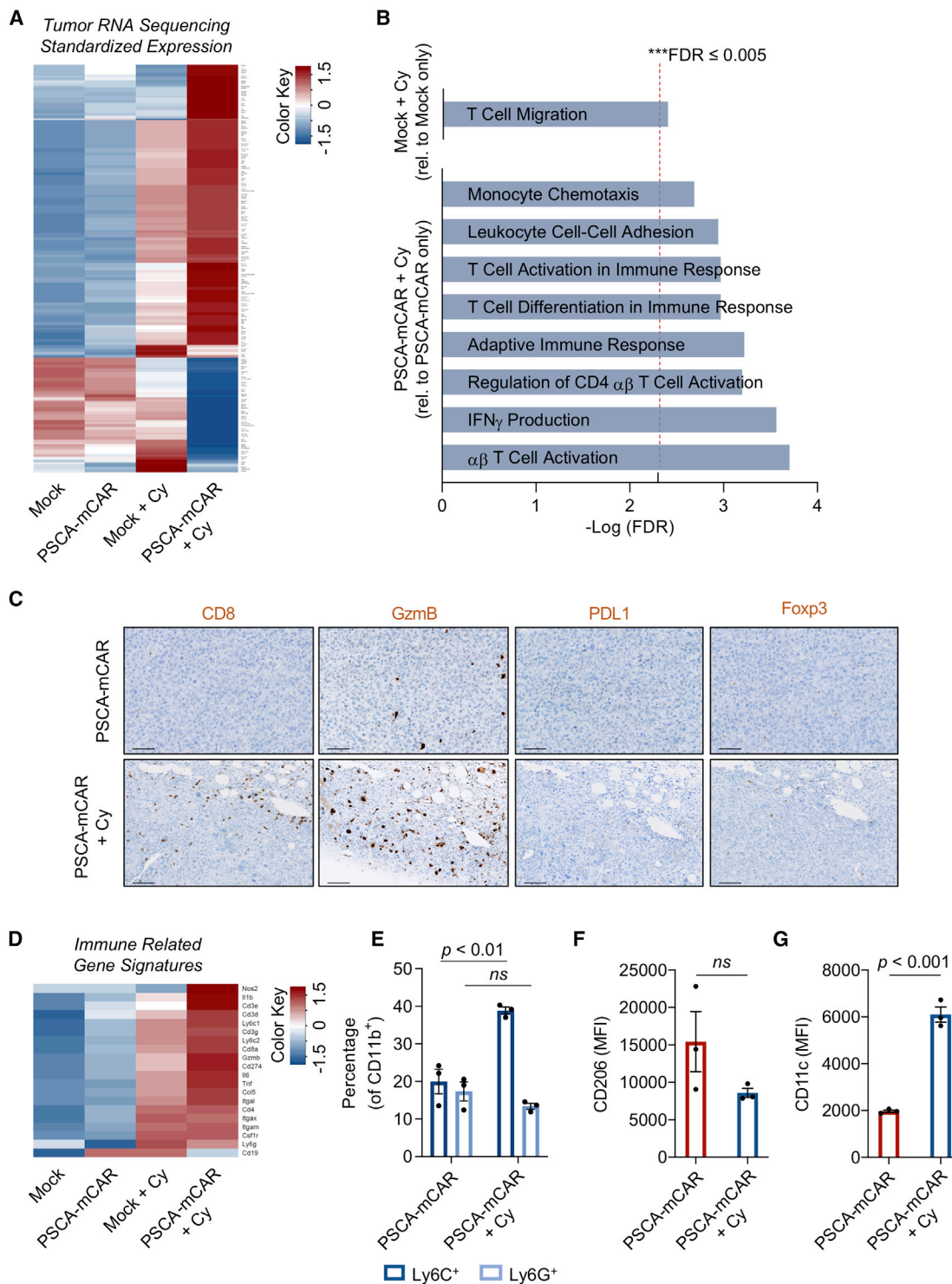
Figure 4. Tumor RNA-seq analysis reveals Cy-mediated pro-inflammatory modulation of the TME

(A) RNA-seq heatmap showing standardized expression of transcripts from RM9-hPSCA tumors after Mock or PSCA-mCAR treatment with or without Cy (100 mg/kg i.p.) pre-conditioning (scale −1.5 to +1.5). (B) GSEA network GO pathway analysis highlighting significant enrichment (FDR ≤ 0.005) in immune-related biological processes from tumors treated with Mock + Cy relative to Mock alone (top) or PSCA-mCAR + Cy treatment relative to PSCA-mCAR alone (bottom). (C) IHC of CD8, GzmB, PD-L1, and Foxp3 in representative tumor tissues treated with PSCA-mCAR T cells alone or PSCA-mCAR following Cy pre-conditioning. 20× magnification; scale bars represent 100 μm. (D)

(legend continued on next page)

post T cell treatment, both failed to show an accumulation of peripheral PSCA-mCAR T cells, despite evidence of a Cy mediated peripheral lymphodepletion (Figure 3E; Figures S7A and S7B). These data highlight a Cy-mediated modulation of the local TME resulting in tumor-specific trafficking and expansion of PSCA-mCAR T cells.

Cy overcomes the immunosuppressive TME

To better understand the impact of Cy on the local TME, we performed RNA sequencing (RNA-seq) of tumors in each treatment group. Analysis of standardized transcript expression revealed that Cy pre-conditioning induced widespread transcriptional changes in comparison to Mock or PSCA-mCAR T cells alone, indicating a local tumor modulating effect of Cy (Figure 4A). A Gene Ontology (GO) Gene Set Enrichment Analysis (GSEA) of biological processes was performed to identify most impacted gene pathways. GSEA analysis showed significant enrichment of T cell migration pathways in tumors following Cy pre-conditioning alone (Figure 4B, top). Tumors from PSCA-mCAR T cells in combination with Cy showed multiple pathway enrichment sets, highlighted by multiple T cell activation pathways, increased IFN-γ production, increased adaptive immune responses, and monocyte chemotaxis (Figure 4B, bottom).

IHC analysis of tumors in each treatment group reflected the observed transcriptional changes, which suggested a favorable pro-inflammatory TME shift allowing a reversion of T cell exclusion (Figure 4C). Specifically, we found increased frequencies of intratumoral cytotoxic CD8$^+$ T cells and a corresponding increase of granzyme-B$^+$ (GzmB) cells following Cy pre-conditioning. We also observed increases in intratumoral PD-L1 in areas coincident with higher T cell accumulation. Interestingly, Cy did not appear to modulate Foxp3$^+$ Treg frequencies within the tumor. Increased immune-related gene signatures in pre-conditioned tumors highlight the impact of Cy, which was further enhanced by the presence of PSCA-mCAR T cells (Figure 4D). The majority of upregulated genes included markers of immune cell subsets (e.g., *Cd3e, Cd4, Cd8a, Itgam*), monocyte/myeloid cell activation/differentiation (e.g., *Ly6c1/2, Ly6g, Csf1r, Itgam/Cd11b, Itgax/Cd11c*), T cell activation (e.g., *Gzmb, Cd274*), pro-inflammatory factors (e.g., *Il6, Nos2, Il1b, Tnf, Il33*), and T cell chemoattraction (e.g., *Ccl5, Cxcl9*). Transcriptional changes to select genes were confirmed using RT-PCR (Figure S8). Flow cytometry analysis of pro-inflammatory monocytic Ly6C$^+$ cells (gated within CD11b$^+$) showed a significant increase following Cy pre-conditioning (Figure 4E). Cy pre-conditioning also resulted in fewer tumor-promoting M2-like CD206$^+$ myeloid cells and increased CD11c$^+$ antigen presenting myeloid populations (Figures 4F and 4G), confirming findings from the RNA-seq analysis. *In silico* interrogation of differentially expressed genes using Ingenuity Pathway Analysis (IPA) showed induction of innate/adaptive immune cell communication canonical pathways following Cy pre-conditioning, with antigen-pre-sentation pathways most upregulated following PSCA-mCAR T cells and Cy (Figures S9A–S9D). Furthermore, a pro-inflammatory shift in peripheral myeloid subsets (increased peripheral Ly6C$^+$ and decrease in Ly6G$^+$) was observed in the blood of mice treated with the combination of Cy pre-conditioning and PSCA-mCAR T cells relative to CAR T cells alone (Figure S9E). Flow cytometry analysis of Ly6C$^+$ and Ly6G$^+$ in the tumor and blood of Mock + Cy treated mice also showed frequency shifts compared to Mock alone, further supporting the Cy-mediated impact on myeloid cell subsets in pre-conditioned mice (Figure S10). Overall, these data support a key role for Cy in overcoming the local immunosuppressive TME and promoting endogenous anti-tumor immunity.

PSCA-mCAR T cells effectively target PSCA$^+$ prostate cancer bone metastases and generate protective tumor immunity

We next assessed our therapy in a more clinically relevant bone metastatic model. hPSCA-KI mice were i.ti. engrafted with RM9-hPSCA tumors, pre-conditioned with Cy, followed by i.v. Mock or PSCA-mCAR T cell treatment as described in Figure 5A. Tumor flux imaging indicated that mice treated with Mock T cells, Mock T cells with Cy, and PSCA-mCAR T cells alone showed minimal anti-tumor responses. In contrast, PSCA-mCAR T cells in combination with Cy pre-conditioning promoted anti-tumor responses in the majority of treated mice (Figure 5B; Figure S11A) with 50% curative responses (Figure 5C). At day 7 post-CAR T cell therapy, we observed clearance of bone tumors and unremarkable gross architecture of bone marrow in the combination group (Figure S11B).

We next examined the impact on long-term anti-tumor immunity resulting from reversion of T cell exclusion observed in mice pre-conditioned with Cy and treated with CAR T cells (Figure 4; Figure S9). Cured mice following Cy and CAR T cell combo treatment, along with tumor naive control mice, were rechallenged with s.c. RM9-hPSCA tumors (Figure 5D, left). Impressively, in mice rechallenged with PSCA-expressing tumor, we observed rejection in 80% of mice as shown by flux imaging and caliper tumor volume measurement (Figure 5D, right, and 5E). Mice rechallenged with RM9-hPSCA failed to show a re-emergence of PSCA-mCAR T cells systemically, suggesting that tumor rejection was independent of PSCA-CAR targeting of PSCA$^+$ tumor and related to modified endogenous anti-tumor immunity (Figure 5F). To confirm this, we repeated rechallenge in Cy and PSCA-mCAR cured mice as before, but this time rechallenged with RM9 wild-type tumors (non-PSCA, non-ffluc expressing) and again saw strong endogenous anti-tumor immunity in mice previously cured with Cy and PSCA-mCAR T cell treatment relative to tumor naive mice (Figure 5G). These data suggest that Cy and CAR T cell-mediated increases in antigen presentation, innate/adaptive immune response, and IFN-γ signaling pathways results in improved

---

Heatmap showing standardized expression of immune related gene signatures from bulk tumors reveal pro-immune shifts following PSCA-mCAR or combo treatment (scale −1.5 to +1.5). (E) Flow cytometry quantification of frequency shifts within intra-tumoral pro-inflammatory Ly6C$^+$ (CD206$^-$F4/80$^+$) or MDSC-like Ly6G$^+$ myeloid cells (gated on CD45$^+$CD11b$^+$) following indicated treatments. (F and G) Quantification of MFI of M2-like macrophage marker CD206 (F) and dendritic cell marker CD11c (G) on tumoral myeloid cells following indicated treatments. For all data, N ≥ 2 mice per group. p values were determined using unpaired Student's t test.
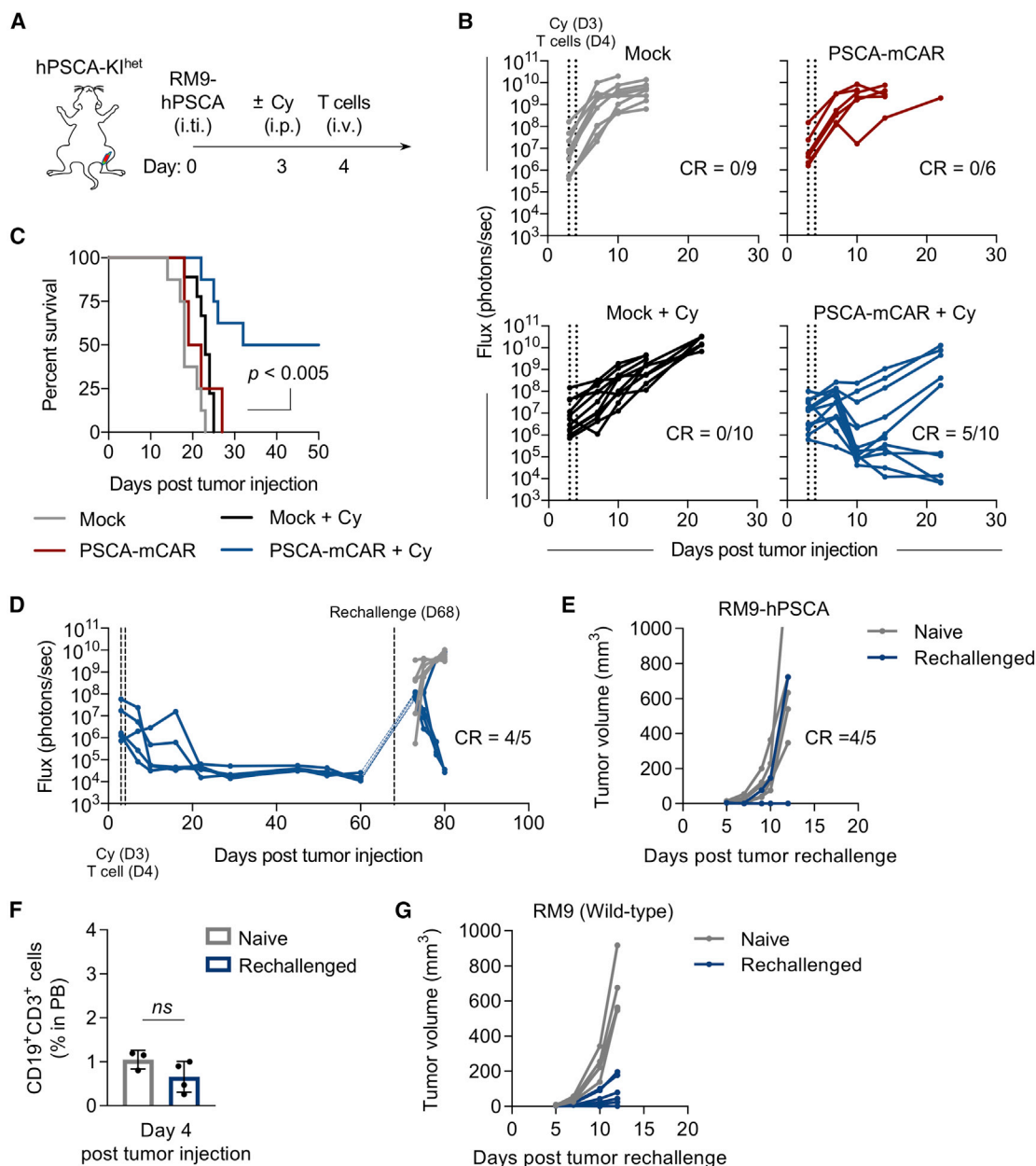
Figure 5. Cy pre-conditioning combined with PSCA-mCAR T cell treatment is effective *in vivo* against bone-metastatic RM9-hPSCA prostate tumors and promotes protective anti-tumor immune memory

(A) Illustration of RM9-hPSCA i.ti. engrafted prostate tumors with or without Cy pre-conditioning (vehicle or Cy 100 mg/kg, i.p.) 24 h prior to treatment with 5.0×10^6 T cells (Mock or PSCA-mCAR, i.v.). (B) Tumor flux in each treatment group as measured by bioluminescent imaging in each replicate mouse at indicated days post tumor injection. (C) Kaplan-Meier survival for treated mice. p value indicates difference between Mock + Cy and PSCA-mCAR + Cy as determined by log rank (Mantel-Cox) test. (D) Tumor flux in mice engrafted with RM9-hPSCA i.ti., which achieved CR following PSCA-mCAR treatment with Cy pre-conditioning. At day 68 post initial tumor injection, tumor naive and previously cured mice were then rechallenged with s.c. RM9-hPSCA tumors. (E) Corresponding replicate RM9-hPSCA tumor volume measurements in tumor naive and rechallenged mice from Figure 5D. (F) Flow cytometry highlighting absence of %CD19$^+$CD3$^+$ (%PSCA-mCAR, gated on CD45$^+$CD3$^+$) in PB at 4 days post RM9-hPSCA tumor challenge in naive or rechallenge in previously cured PSCA-mCAR + Cy mice. N $\geq$ 3 for PB flow analysis data. Determination of statistical significance between naive and rechallenged conditions was done using an unpaired Student's t test. (G) Replicate RM9 wild-type tumor volume measurements in tumor naive and rechallenged mice previously cured by PSCA-mCAR T cell + Cy treatment. Unless otherwise stated, N $\geq$ 5 mice per group. All data are representative of two independent experiments.
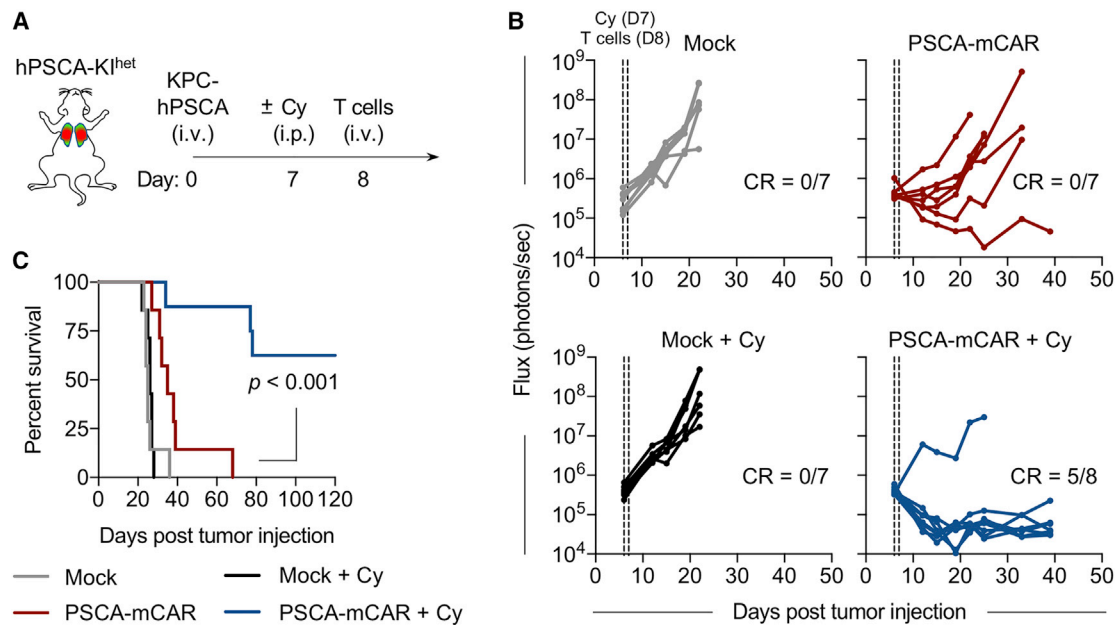
Figure 6. Cy pre-conditioning combined with PSCA-mCAR T cell treatment is effective *in vivo* against PSCA⁺ pancreatic tumor models

(A) Illustration of KPC-hPSCA i.v. engrafted pancreatic tumors established in the lungs, with or without Cy pre-conditioning (vehicle or Cy 100 mg/kg, i.p.) 24 h prior to treatment with 5.0×10^6 T cells (Mock or PSCA-mCAR, i.v.). (B) Tumor flux in each treatment group as measured by bioluminescent imaging in each replicate mouse at indicated days post tumor injection. (C) Kaplan-Meier survival plot for mice in each group indicated. p value indicates difference between PSCA-mCAR and PSCA-mCAR + Cy as determined by log rank (Mantel-Cox) test. For all data shown, N ≥ 7 mice per group. All data are representative of two independent experiments.

primary PSCA-mCAR T cell responses, as well as a stimulation of endogenous protective immunity following tumor rechallenge.

PSCA-mCAR T cells effectively target PSCA⁺ KPC metastatic pancreatic cancer

In addition to its overexpression in prostate cancers and their metastases, PSCA is also highly expressed in pancreatic cancers.[18] Accordingly, we sought to validate our Cy pre-conditioning in combination with PSCA-CAR T cells against KPC pancreatic ductal adenocarcinoma (PDAC) tumor cells engineered to express hPSCA (KPC-hPSCA). Importantly, KPC tumors harbor features of PDAC, including intraepithelial neoplasia and a robust inflammatory reaction including exclusion of effector T cells.[19] KPC-hPSCA were administered i.v., which induces lung metastasis, and were pre-conditioned with Cy, followed with i.v. Mock or PSCA-mCAR T cell treatment as indicated in Figure 6A. Quantification of tumor flux post T cell treatment showed that mice treated with Mock T cells alone or Mock T cells with Cy exhibited minimal anti-tumor responses (Figure 6B; Figure S12A) as expected. Interestingly, PSCA-mCAR T cells treatment alone in this model showed pronounced but transient anti-tumor activity, distinct from the prostate tumor model. Impressively, the combination of Cy pre-conditioning and PSCA-mCAR T cells showed a more potent anti-tumor activity resulting in extended survival and curative responses in over 60% of mice (Figure 6C). IHC of lung tissues at 13 days post-T cell treatment showed disease-free mice treated with PSCA-mCAR T cells and Cy (Figure S12B). Combined, these models demonstrate the utility of pre-

conditioning with Cy to improve PSCA-CAR T cell therapy responses in solid tumors.

DISCUSSION

In this study, we investigated the safety and efficacy of PSCA CAR T cell therapy using immunocompetent hPSCA-KI mice. We discovered that robust local intratumoral activity, proliferation, and therapeutic responses of PSCA-CAR T cells were dependent on pre-conditioning with Cy. PSCA-CAR T cell therapy demonstrated safety in mice with physiological hPSCA expression in normal tissues, mimicking patterns of expression found in humans.[16,17] We showed a lack of therapeutic responses with PSCA-CAR T cell treatment alone in this system, contrasting with the CRs previously observed using human xenograft tumor models in immunocompromised NSG mice.[10] The dramatic improvement of CAR T cell activity and survival of mice following Cy pre-conditioning led us to postulate that in addition to its conventional lymphodepleting effects, Cy also mediates substantial modulation of the solid tumor TME. Accordingly, we showed that Cy pre-conditioning resulted in (1) rapid CAR and endogenous T cell infiltration within the tumor; (2) a TME re-shaping of the myeloid cells from M2 to M1 phenotypes; (3) increases in endogenous antigen presentation pathways; and (4) increases in innate/adaptive immune response signaling, all of which were further enhanced in combination with CAR T cells. Importantly, we also showed CAR antigen-independent protective immunity against tumor rechallenge in this model. Together, these data emphasize three important features: (1) commonly used immunocompromised xenograft animal models

greatly underrepresent the impact of the host immune system thereby overestimating CAR T cell activity, (2) independent of peripheral lymphodepleting effects, Cy modulates the local TME and may be critical to unleashing the full potential of solid tumor CAR T cell therapies, and (3) the combination of Cy pre-conditioning along with CAR T cell therapy in our models also modifies host immunity to elicit protection against tumor rechallenge.

Prior studies have demonstrated that Cy-mediated depletion of peripheral T cells, particularly Tregs, may act as a cytokine sink to alter CD8 T cell activity.[7,20,21] Studies suggest that Cy-mediated depletion of Tregs is highly transient, and modulation of dendritic cell function within the TME may explain improved anti-tumor immunity.[22] Similarly, we did not observe striking changes in tumoral Foxp3$^+$ Tregs following Cy in our model, suggesting alternative modifications of the local TME. We found that as early as 24 h following PSCA-mCAR T cell treatment, clear intratumoral trafficking and accumulation of CAR T cells were observed in Cy pre-conditioned mice. This robust tumoral recruitment of PSCA-mCAR T cells was observed prior to the peak peripheral lymphodepleting effects of Cy in this model. Once maximal lymphodepletion was achieved 3 days following T cell treatment, we then observed great increases in intratumoral T cell expansion both in antigen specific PSCA-mCAR, and to a lesser degree in adoptively transferred non-targeting Mock T cells. This contrasts with previous findings that indicate that intratumoral T cell homing or migration aided by Cy is reserved for antigen-specific T cells.[23] In addition to the direct T cell modulating effects of Cy, pre-conditioning lymphodepletion enhances IL-2, IL-7, and IL-15 cytokine signaling to improve systemic persistence of CD19-CAR T cells.[23,24] However, we found no increases in peripheral CAR T cells despite robust local anti-tumor responses. Additionally, prior to maximal peripheral lymphodepletion, Cy modified the local TME, improving infiltration of endogenous T cells, IFN-γ signaling in the TME, and an M2-like to M1-like macrophage shift. This result is consistent with prior work showing pro-inflammatory modulation by Cy in the TME, which may synergize with type-I IFN cytokines, which we observe especially in combination with antigen-specific PSCA-mCAR T cells.[25,26]

Cy pre-conditioning greatly enhanced PSCA-mCAR T cell activity in the immunocompetent models we tested but did not demonstrate curative responses in all treated mice. This implies that additional CAR T cell resistance mechanisms may limit maximal therapeutic benefits of this approach and must be investigated further. Major resistance mechanisms include hampered T cell trafficking or persistence in tumors, intrinsic and/or acquired resistance to CAR T cell therapy driven in part by immune suppressive pathways, and tumor antigen escape from single-antigen targeted CAR T cell strategies. With regards to trafficking, it is possible that a lack of immediate antigen engagement by systemically administered CAR may limit peripheral survival and trafficking to solid tumors as there is observed trapping of adoptively transferred T cells in first-pass tissues, including lung and liver.[27] Interestingly, PSCA-mCAR T cells, both with and without pre-conditioning, demonstrated greater therapeutic activity in the

lung metastatic KPC-PDAC model, perhaps taking advantage of earlier lung trafficking of systemically administered T cells. A recent study in a melanoma model showed that lymphodepleting chemotherapy pre-conditioning promoted peripheral immunosuppressive MDSCs, which limited persistence of tumor infiltrating T cells and resulted in greater disease progression.[28] While at later time points, Cy-mediated immunosuppression may contribute to tumor recurrences, our data strongly support the early benefits of Cy pre-conditioning in re-shaping the TME to promote CAR T cell responses.

Further studies are warranted to determine the mechanism(s) responsible for the protective immunity following Cy and PSCA-CAR T cell therapy. Immune checkpoint pathways may also limit therapeutic responses and have been highlighted in multiple preclinical and clinical CAR T cell programs.[4,29] In support of this acquired tumor resistance mechanism, we observed robust *in vitro* and *in vivo* induction of PD-1/PD-L1 signaling following PSCA-CAR T cell treatment.[30–32] Future studies will investigate the benefits of combining PSCA-CAR T cells with immune checkpoint blockade and other acquired or intrinsic immunosuppressive pathways. While Cy pre-conditioning prior to CAR T cell therapy may overcome some of the obstacles in solid tumors, this regimen may not address other tumor-resistance mechanisms that further challenge CAR T cell activity, including tumor antigen heterogeneity and antigen escape.[33–35] In our model, tumor cells were clonally positive or fluorescence-activated cell sorted (FACS) for uniformly positive PSCA expression, which would greatly reduce the possibility of an antigen-negative outgrowth following CAR T cell therapy. However, transcriptional downregulation or novel PSCA mutations in response to CAR T cell pressure may have occurred, similar to clinical observations following CD19-CAR T cell therapy.[33,36] Prior clinical experience with hematological malignancies and solid tumors alike suggests antigen heterogeneity is likely a key barrier that will require multi-targeted CAR T cell approaches.

To our knowledge, this is the first example of a preclinical model to assess the safety of PSCA-targeted agents, including CAR T cell therapy. Several groups have developed immunocompetent mouse models to evaluate the safety of T cell therapeutic approaches, including those targeting CD19, CEA, and HER2.[14,37,38] In pre-clinical CD19-CAR T cell models, the severity of toxicity (i.e., CRS, neurotoxicity, and in some cases death) was increased in the presence of lymphodepleting pre-conditioning regimens.[39] Further, in human CEA transgenic mouse models, it was found that CEA-targeted CAR T cells were only effective when combined with lymphodepletion. In these mice, toxicities (colitis, weight loss, liver toxicity, and death) were only seen in mice pre-conditioned with total body irradiation (TBI) alone or a triple combination of fludarabine, Cy, and TBI.[14,40] In contrast, tumor-bearing hPSCA-KI mice who received Cy preconditioning and PSCA-CAR T cell therapy displayed no overt toxicities, including normal tissues expressing PSCA; however, expression intensity and pattern of PSCA in our hPSCA-KI model may not completely represent human biology. Our phase 1 clinical trial (ClinicalTrials.gov: NCT03873805) is evaluating the safety, feasibility, and biological activity of PSCA-CAR T cells in patients with mCRPC, and based on these

preclinical studies we have added a lymphodepletion arm to assess the effects on the TME and clinical outcomes.

MATERIALS AND METHODS

Cell lines

The Ras/Myc transformed prostate cancer line, RM9 and ffluc expressing LSL-Kras$^{G12D/+}$, LSL-Trp53$^{R172H/+}$, Pdx-1-Cre (KPC), and ID8 cell lines were a kind gift from Drs. Timothy C. Thompson at MD Anderson Cancer Center, Edwin Manuel, and Karen Aboody at City of Hope, respectively.[41,42] Cell lines were cultured in Dulbecco's modified Eagle's medium (Life Technologies), containing 10% fetal bovine serum (FBS, Hyclone), 25 mM HEPES (Irvine Scientific), 2 mM L-Glutamine (Fisher Scientific), and 1X antibiotic-antimycotic (1X AA, GIBCO; cDMEM). PLAT-E retroviral packaging cells (Cell Biolabs) were cultured in cDMEM with addition of 1 μg/mL puromycin and 10 μg/mL blasticidin (InvivoGen) prior to transfection. All cells were cultured at 37°C with 5% CO_2.

Animals

Animal experiments were performed under protocols approved by the City of Hope Institutional Animal Care and Use Committee. For all *in vivo* studies, 6- to 8-week-old male mice were used. hPSCA-KI C57BL/6j mice, whose generation has been described previously, were provided by Drs. Robert E. Reiter and Anna Wu at UCLA.[16] To prevent possible rejection of tumor lines that endogenously express murine PSCA, we F1 crossed homozygous hPSCA-KI mice with wild-type C57BL/6j mice to generate heterozygous hPSCA-KI mice. Unless otherwise indicated, all mice used in experiments were heterozygous hPSCA-KI. For experiments in immunocompromised animals, 6- to 8-week-old RAG2$^{-/-}$ (Jackson Laboratories) mice were used.

Genotyping PCR

To confirm the genotype of hPSCA-KI mice, we isolated and analyzed genomic DNA by PCR. Genomic DNA was collected from tail or ear tissue isolated via QIAGEN DNA Mini Kit (QIAGEN) according to the manufacturer's protocol. Isolated DNA samples were analyzed in independent master mixes containing primers, Accustart PCR SuperMix (Quantabio), and sterile DNase/RNase-free water. Three primer sequences (kindly provided by Dr. Robert Reiter at UCLA) were used to detect murine genomic PSCA DNA (from 5′ and 3′ arms) and hPSCA cDNA as follows: mPSCA-5′ arm primer sequence, 5′-TGTCACTGTT-GACTGTGGGTAGCA-3′; mPSCA-3′ arm primer sequence, 5′-CTTACTTGATAGGAGGGCTCAGCA-3′; hPSCA primer sequence, 5′-CCAGAGCAGCAGGCCGAGTGCA-3′. PCR was performed on a FlexCycler^2 (Analytik Jena) programmed for 94°C for 1 min, 35 cycles at (94°C for 20 s, 59°C for 20 s, 72°C for 45 s), and a final run at 72°C for 3 min. PCR products were loaded on to 2% agarose gels, run at 150 V for approximately 20 min, and stained in SybrSafe (Life Technologies) prior to imaging on a BioSpectrum MultiSpectral Imaging System (UVP).

DNA constructs, tumor lentiviral transduction, and retrovirus production

Tumor cells were engineered to express ffluc and tumor antigen hPSCA by sequential transduction with epHIV7 lentivirus carrying the ffluc gene under the control of the EF1α promoter, and epHIV7 lentivirus carrying the hPSCA gene under the control of the EF1α promoter as described previously.[10] The scFv sequence from the murine anti-hPSCA antibody clone (1G8) was used to develop the mCAR construct.[43] The extracellular spacer domain included the murine CD8 hinge region followed by a murine CD8 transmembrane domain.[44,45] The intracellular co-stimulatory signaling domain contained the murine 4-1BB followed by a murine CD3ζ cytolytic domain as previously described.[46] The CAR sequence was separated from a truncated murine CD19 gene (mCD19t) by a T2A ribosomal skip sequence and cloned into the pMYs retrovirus backbone (Cell Biolabs). Production of retrovirus used to transduce primary murine T cells was performed as previously described.[47] The CAR sequence was separated from a truncated murine CD19 gene (mCD19t) by a T2A ribosomal skip sequence and cloned into the pMYs retrovirus backbone under the control of a hybrid MMLV/MSCV promoter (Cell Biolabs). NT-mCAR cells were similar to PSCA-mCAR in the pMYs retrovirus backbone but incorporated an scFv targeting a non-PSCA antigen. The ffluc sequence was also cloned into the pMYs retrovirus backbone. Retrovirus was produced by transfecting the ecotropic retroviral packaging cell line, PLAT-E, with addition of PSCA-mCAR, NT-mCAR, or ffluc retrovirus backbone plasmid DNA using FuGENE HD transfection reagent (Promega). Viral supernatants were collected after 24, 36, and 48 h, pooled, and stored at −80°C in aliquots for future T cell transductions.

Murine T cell isolation, transduction, and *ex vivo* expansion

Splenocytes were obtained by manual digestion of spleens from male heterozygous hPSCA-KI mice. Enrichment of T cells was performed by EasySep mouse T cell isolation kit per manufacturer's protocol (StemCell Technologies). Retroviral transduction with PSCA-mCAR, NT-mCAR, and/or ffluc and subsequent expansion were performed as previously described.[47]

Flow cytometry

Flow cytometric analysis was performed as previously described.[10,47] Briefly, cells were resuspended in Hank's balanced salt solution without Ca^{2+}, Mg^{2+}, or phenol red (HBSS$^{-/-}$, Life Technologies) containing 2% FBS and 1× AA (GIBCO; FACS buffer). Single cell suspensions from mouse tissues or tumors were incubated for 15 min at ambient room temperature with rat anti-mouse Fc Block (BD PharMingen). Cells were then incubated with primary antibodies for 30 min at 4°C in the dark. For secondary staining, cells were washed twice prior to 30 min incubation at 4°C in the dark with either Brilliant Violet 510 (BV510), fluorescein isothiocyanate (FITC), phycoerythrin (PE), peridinin chlorophyll protein complex (PerCP), PerCP-Cy5.5, PE-Cy7, allophycocyanin (APC), or APC-Cy7 (or APC-eFluor780)-conjugated antibodies. Anti-mouse antibodies against mCD206 (BioLegend, clone: C068C2), mLy6G (BioLegend, clone: 1A8), mLy6C (BioLegend, clone: HK1.4), mCD11b (BioLegend, clone: M1/70), mCD11c (BioLegend, clone: N418), mMHC class II (I-A/I-E, BioLegend, clone: M5/144.15.2), mCD274 (mPD-L1, BioLegend, clone:10F.9G2), mCD45

(BioLegend, clone: 30-F11), mCD19 (BD Biosciences, clone: 1D3), mCD3 (BioLegend, clone: 17A2), mCD279 (mPD-1, BioLegend, clone: 29F.1A12), mCD4 (BioLegend, clone: RM4-5), mCD137 (Thermo Fisher, clone: 17b5), mCD8a (Miltenyi Biotec, clone: 53-6.7), mCD44 (BD Biosciences, clone: IM7), mCD62L (BioLegend, clone: MEL-14), mCCR7 (Thermo Fisher, clone: 4B12), biotinylated Protein L (GenScript USA), PE conjugated streptavidin (SA-PE; BD Biosciences), and goat anti-mouse immunoglobulin (Ig; BD Biosciences) were used for flow cytometry. Additionally, a mouse anti-hPSCA antibody (clone 1G8) used for flow cytometry was from the laboratory of Dr. Robert Reiter at UCLA.[17] Cell viability was determined using 4', 6-diamidino-2-phenylindole (DAPI, Sigma). Flow cytometry was performed on a MACSQuant Analyzer 10 (Miltenyi Biotec), and data was analyzed with FlowJo software (v10, TreeStar).

In vitro tumor killing and T cell functional assays

For tumor killing assays, PSCA-mCAR T cells and tumor targets were co-cultured at indicated E:T ratios in the absence of exogenous cytokines or antibiotics in 96-well plates for 24 to 72 h and analyzed by flow cytometry. Tumor killing was calculated by comparing DAPI-negative (viable) mCD45-negative cell counts in co-cultures with CAR T cells relative to that observed in co-culture with Mock (untransduced) T cells. T cell functional analysis from these assays was also determined by flow cytometry, using indicated cell surface antibodies.

ELISA cytokine assays

Cell-free supernatants from tumor killing assays were collected at indicated times and frozen at $-20°C$ for further analysis. Murine IFN-γ and IL-2 cytokines were measured in supernatants according to the murine IFN-γ and IL-2 ELISA Ready-SET-GO! ELISA kit (Invitrogen) according to the manufacturer's protocol, respectively. Plates were read at 450 nm using a Cytation3 imaging reader with Gen5 microplate software v3.05 (BioTek).

Tumor RNA isolation, sequencing, and analysis

Tumor tissue samples harvested from mice were immediately snap-frozen in liquid nitrogen and stored at $-80°C$ for further processing. Frozen tumor samples were placed in Green RINO RNA lysis tubes for bead homogenization in a Bullet Blender homogenizer (Next Advance) in the presence of TRIzol at 4°C. Lysate was then chloroform extracted for RNA and purified via a QIAGEN RNA Easy isolation kit (QIAGEN) according to the manufacturer's protocol. Libraries for stranded poly(A) RNA-seq were created using the KAPA mRNA HyperPrep kit (Roche).

Sequencing of 51 bp single-end reads was performed using a HiSeq2500 regular run. Base calling (de-multiplexing samples between and within labs by 6 bp barcodes, from a 7 bp index read) was performed using bcl2fastq v2.18. Reads were aligned against the mouse genome (mm10) using TopHat2[48]. Read counts were tabulated using htseq-count,[49] with UCSC known gene annotations (TxDb.Mmusculus.UCSC.mm10.knownGene, downloaded 8/30/2018).[50] Fold-

change values were calculated from fragments per kilobase per million (FPKM) reads normalized expression values, which were also used for visualization (following a $\log_2$ transformation).[51] Aligned reads were counted using GenomicRanges.[52] Scripts are a modified version of a template for RNA-seq gene expression analysis (https://github.com/cwarden45/RNAseq_templates/tree/master/TopHat_Workflow) and RNA-seq data for this study was deposited in NCBI's Gene Expression Omnibus (GEO) with GEO: GSE165197, GSM5028084, GSM5028085, GSM5028086, and GSM5028087. Expression of $\log_2$(FPKM + 0.1) expression was visualized in heatmaps using heatmap.3 (https://github.com/obigriffith/biostar-tutorials/blob/master/Heatmaps/heatmap.3.R). Custom gene sets defined in IPA (Ingenuity Systems, https://digitalinsights.qiagen.com/) was used for generation of specific heatmap gene sets used in the current study. Candidate genes were selected by pairwise comparisons between treatment groups, looking for genes with a |fold-change| >1.5. Genes were filtered to only include transcripts with an FPKM expression level of 1 (after additional rounding during $\log_2$-transformation) in at least 50% of samples, as well as genes that are greater than 150 bp. An expression level of FPKM greater than 1 was used to reduce false positives. Expression level FPKM data was then used to generated 1 versus 1 treatment group comparisons. IPA pathway analysis was used to calculate canonical pathway enrichments among treatment groups and generation of heatmaps using the provided set of genes. GSEA was run on $\log_2$(FPKM + 0.1) expression values, with upregulated enrichment results for GO Biological Process categories in MSigDB.[53–55]

RT-PCR

cDNA was prepared from 1µg of total RNA (matched from RNA-seq analyses) using SuperScript IV reverse transcriptase (Thermo Fisher). Quantitative PCR was performed in triplicate using pooled cDNA samples per treatment group (N $\geq$ 2 mice per group) using SsoAdvanced Universal SYBR Green Supermix (BioRad). Data were analyzed by the comparative threshold method, and gene expression was normalized to GAPDH expression. Murine forward (F) and reverse (R) gene primer sequences used for RT-PCR analysis in this study are included in Table S1.

In vivo tumor studies

For in vivo i.ti. tumor studies, 2.5×10^4 RM9-hPSCA/ffluc cells were prepared HBSS$^{-/-}$ and i.ti. engrafted in 6- to 8-week-old male heterozygous hPSCA-KI mice as described previously.[10] For in vivo s.c. tumor studies, $0.2–1.0 \times 10^6$ RM9-hPSCA/ffluc cells were prepared in HBSS$^{-/-}$ and s.c. engrafted in 6- to 8-week-old male heterozygous hPSCA-KI mice. Tumor growth was monitored at least twice per week via biophotonic imaging (LagoX, Spectral Instruments) or by volumetric caliper measurement (length $\times$ width $\times$ height = mm^3). Flux signals were analyzed by noninvasive optimal imaging as previously described.[10,47] For i.ti. studies, on day 3 or 4 post engraftment, mice were grouped based on flux signal and i.p. injected with the indicated dose of Cy (Sigma-Aldrich) or vehicle (sterile PBS). For s.c. studies, mice were treated i.p. with Cy at 100 mg/kg unless otherwise specified or vehicle once tumor volumes reached an average of 100 mm^3. For all studies, mice received i.v. treatment with 5.0×10^6

Mock, NT-mCAR, or PSCA-mCAR T cells as specified. Flux imaging or caliper measurement continued until scheduled harvest or humane endpoints were reached. For tumor rechallenge studies, tumor burden was measured by flux imaging until CRs were achieved and maintained for at least 30 days. Mice achieving a CR and age-matched tumor naive hPSCA-KI control mice were then rechallenged by s.c. injection of 0.5 to 1.0×10^5 RM9-hPSCA/ffluc or RM9 wild-type (non-PSCA, non-ffluc) cells and engraftment was measured by flux imaging and/or volumetric caliper measurement. Humane endpoints were used in determining survival. Mice were euthanized upon reaching i.ti. and s.c. tumor volumes in excess of 1,500 mm^3, showing signs of distress, labored or difficulty breathing, weight loss, impaired mobility, or evidence of being moribund.

PB was collected from isoflurane-anesthetized mice by retro-orbital (RO) bleed through heparinized capillary tubes (Chase Scientific) into polystyrene tubes containing a heparin/PBS solution (1,000 U/mL, Sagent Pharmaceuticals) at the indicated time points. Volume of each RO blood draw was recorded for cell quantification per μL blood. Tumor and normal tissue samples harvested from euthanized mice were collected into ice-cold PBS and subsequently processed using a murine tumor digestion kit (Miltenyi Biotec) according to the manufacturer's protocol. Red blood cells (RBCs) from either RO bleed or tissue collection were lysed with 1X Pharmlyse buffer (BD Biosciences) according to the manufacturer's protocol and then washed, stained, and analyzed by flow cytometry.

IHC and RNA *in situ* hybridization
Tumor tissue was fixed in 4% paraformaldehyde (4% PFA, Boston BioProducts) and stored in 70% ethanol until further processing. IHC was performed by the Research Pathology Core at City of Hope. Briefly, paraffin sections (5 μm) were stained with hematoxylin and eosin (H&E, Sigma-Aldrich), mouse anti-hPSCA antibody (Abnova, H00008000-M03, clone: 5C2), anti-mouse CD3 (Abcam, ab16669, clone: SP7), anti-mouse GzmB (Abcam, ab4059, polyclonal), anti-mouse CD8a (Cell Signaling, 98941S, clone: D4W2Z), anti-mouse PD-L1 (Abcam, AB80276, clone: MIH6), and anti-mouse FOXP3 (Abcam, clone: EPR22102-37) according to the manufacturer's protocol. RNA *in situ* hybridization of hPSCA was performed by RNAScope (ACD). Images were obtained using the Nanozoomer 2.0HT digital slide scanner and the associated NDP.view2 software (Hamamatsu).

Statistical analysis
Data are presented as mean ± standard error of the mean (SEM) unless otherwise stated. Statistical comparisons between groups were performed using the unpaired two-tailed Student's t test to calculate p value unless otherwise stated. ns, not significant.

Availability of Data
All data associated with this study are present in the paper or the Supplemental information. Materials are available from S.J.P. under a material transfer agreement with City of Hope.

SUPPLEMENTAL INFORMATION
Supplemental Information can be found online at https://doi.org/10.1016/j.ymthe.2021.02.024.

AUTHOR CONTRIBUTIONS
J.P.M. provided conception and construction of the study, provided manuscript writing and editing, and performed the majority of experimental procedures and data analysis. S.J.P. provided conception, construction, and supervision of the study and manuscript writing and editing. D.T., A.K.P., L.S.L., C.A.Y., J.G., Y.Y., H.J.L., K.T.K., B.J.G., and W.-C.C. contributed to experimental procedures and/or data analysis. R.E.R. and C.P.T. provided access to transgenic mice and were consulted on related studies. C.M., A.M.W., R.E.R., T.B.D., and S.J.F. were consulted on methodologies and/or assisted in manuscript writing and editing.

DECLARATION OF INTERESTS
S.J.P. and S.J.F. are scientific advisors to and receive royalties from Mustang Bio. All other authors declare no competing interests.

REFERENCES
1. Wang, Z., Chen, W., Zhang, X., Cai, Z., and Huang, W. (2019). A long way to the battlefront: CAR T cell therapy against solid cancers. J. Cancer 10, 3112–3123.

2. Priceman, S.J., Forman, S.J., and Brown, C.E. (2015). Smart CARs engineered for cancer immunotherapy. Curr. Opin. Oncol. 27, 466–474.

3. Mardiana, S., Solomon, B.J., Darcy, P.K., and Beavis, P.A. (2019). Supercharging adoptive T cell therapy to overcome solid tumor-induced immunosuppression. Sci. Transl. Med. 11, eaaw2293.

4. Bonaventura, P., Shekarian, T., Alcazer, V., Valladeau-Guilemond, J., Valsesia-Wittmann, S., Amigorena, S., Caux, C., and Depil, S. (2019). Cold Tumors: A Therapeutic Challenge for Immunotherapy. Front. Immunol. 10, 168.

5. Fleming, V., Hu, X., Weber, R., Nagibin, V., Groth, C., Altevogt, P., Utikal, J., and Umansky, V. (2018). Targeting Myeloid-Derived Suppressor Cells to Bypass Tumor-Induced Immunosuppression. Front. Immunol. 9, 398.

6. Muranski, P., Boni, A., Wrzesinski, C., Citrin, D.E., Rosenberg, S.A., Childs, R., and Restifo, N.P. (2006). Increased intensity lymphodepletion and adoptive immunotherapy–how far can we go? Nat. Clin. Pract. Oncol. 3, 668–681.

7. Gattinoni, L., Finkelstein, S.E., Klebanoff, C.A., Antony, P.A., Palmer, D.C., Spiess, P.J., Hwang, L.N., Yu, Z., Wrzesinski, C., Heimann, D.M., et al. (2005). Removal of homeostatic cytokine sinks by lymphodepletion enhances the efficacy of adoptively transferred tumor-specific CD8+ T cells. J. Exp. Med. 202, 907–912.

8. Mikyskova, R., Indrova, M., Pollakova, V., Bieblova, J., Simova, J., and Reinis, M. (2012). Cyclophosphamide-induced myeloid-derived suppressor cell population is immunosuppressive but not identical to myeloid-derived suppressor cells induced by growing TC-1 tumors. J. Immunother. 35, 374–384.

9. Bracci, L., Schiavoni, G., Sistigu, A., and Belardelli, F. (2014). Immune-based mechanisms of cytotoxic chemotherapy: implications for the design of novel and rationale-based combined treatments against cancer. Cell Death Differ. 21, 15–25.

10. Priceman, S.J., Gerdts, E.A., Tilakawardane, D., Kennewick, K.T., Murad, J.P., Park, A.K., Jeang, B., Yamaguchi, Y., Yang, X., Urak, R., et al. (2017). Co-stimulatory signaling determines tumor antigen sensitivity and persistence of CAR T cells targeting PSCA+ metastatic prostate cancer. OncoImmunology 7, e1380764.

11. Gu, Z., Thomas, G., Yamashiro, J., Shintaku, I.P., Dorey, F., Raitano, A., Witte, O.N., Said, J.W., Loda, M., and Reiter, R.E. (2000). Prostate stem cell antigen (PSCA) expression increases with high gleason score, advanced stage and bone metastasis in prostate cancer. Oncogene 19, 1288–1296.

12. Reiter, R.E., Gu, Z., Watabe, T., Thomas, G., Szigeti, K., Davis, E., Wahl, M., Nisitani, S., Yamashiro, J., Le Beau, M.M., et al. (1998). Prostate stem cell antigen: a cell surface marker overexpressed in prostate cancer. Proc. Natl. Acad. Sci. USA 95, 1735–1740.

13. Semenkow, S., Li, S., Kahlert, U.D., Raabe, E.H., Xu, J., Arnold, A., Janowski, M., Oh, B.C., Brandacher, G., Bulte, J.W.M., et al. (2017). An immunocompetent mouse model of human glioblastoma. Oncotarget 8, 61072–61082.

14. Wang, J., Ma, N., Okamoto, S., Amaishi, Y., Sato, E., Seo, N., Mineno, J., Takesako, K., Kato, T., and Shiku, H. (2016). Efficient tumor regression by adoptively transferred CEA-specific CAR-T cells associated with symptoms of mild cytokine release syndrome. OncoImmunology 5, e1211218–e1211218.

15. Sckisel, G.D., Mirsoian, A., Minnar, C.M., Crittenden, M., Curti, B., Chen, J.Q., Blazar, B.R., Borowsky, A.D., Monjazeb, A.M., and Murphy, W.J. (2017). Differential phenotypes of memory CD4 and CD8 T cells in the spleen and peripheral tissues following immunostimulatory therapy. J. Immunother. Cancer 5, 33.

16. Zhang, M., Kobayashi, N., Zettlitz, K.A., Kono, E.A., Yamashiro, J.M., Tsai, W.K., Jiang, Z.K., Tran, C.P., Wang, C., Guan, J., et al. (2019). Near-Infrared Dye-Labeled Anti-Prostate Stem Cell Antigen Minibody Enables Real-Time Fluorescence Imaging and Targeted Surgery in Translational Mouse Models. Clin. Cancer Res. 25, 188–200.

17. Gu, Z., Yamashiro, J., Kono, E., and Reiter, R.E. (2005). Anti-prostate stem cell antigen monoclonal antibody 1G8 induces cell death in vitro and inhibits tumor growth in vivo via a Fc-independent mechanism. Cancer Res. 65, 9495–9500.

18. Katari, U.L., Keirnan, J.M., Worth, A.C., Hodges, S.E., Leen, A.M., Fisher, W.E., and Vera, J.F. (2011). Engineered T cells for pancreatic cancer treatment. HPB (Oxford) 13, 643–650.

19. Lee, J.W., Komar, C.A., Bengsch, F., Graham, K., and Beatty, G.L. (2016). Genetically Engineered Mouse Models of Pancreatic Cancer: The KPC Model (LSL-Kras(G12D/+) ;LSL-Trp53(R172H/+) ;Pdx-1-Cre), Its Variants, and Their Application in Immuno-oncology Drug Discovery. Curr. Protoc. Pharmacol. 73, 14.39.11–14.39.20.

20. Scurr, M., Pembroke, T., Bloom, A., Roberts, D., Thomson, A., Smart, K., Bridgeman, H., Adams, R., Brewster, A., Jones, R., et al. (2017). Low-Dose Cyclophosphamide Induces Antitumor T-Cell Responses, which Associate with Survival in Metastatic Colorectal Cancer. Clin. Cancer Res. 23, 6771–6780.

21. Lutsiak, M.E.C., Semnani, R.T., De Pascalis, R., Kashmiri, S.V.S., Schlom, J., and Sabzevari, H. (2005). Inhibition of CD4(+)25+ T regulatory cell function implicated in enhanced immune response by low-dose cyclophosphamide. Blood 105, 2862–2868.

22. Radojcic, V., Bezak, K.B., Skarica, M., Pletneva, M.A., Yoshimura, K., Schulick, R.D., and Luznik, L. (2010). Cyclophosphamide resets dendritic cell homeostasis and enhances antitumor immunity through effects that extend beyond regulatory T cell elimination. Cancer Immunol. Immunother. 59, 137–148.

23. Bracci, L., Moschella, F., Sestili, P., La Sorsa, V., Valentini, M., Canini, I., Baccarini, S., Maccari, S., Ramoni, C., Belardelli, F., and Proietti, E. (2007). Cyclophosphamide enhances the antitumor efficacy of adoptively transferred immune cells through the induction of cytokine expression, B-cell and T-cell homeostatic proliferation, and specific tumor infiltration. Clin. Cancer Res. 13, 644–653.

24. Ninomiya, S., Narala, N., Huye, L., Yagyu, S., Savoldo, B., Dotti, G., Heslop, H.E., Brenner, M.K., Rooney, C.M., and Ramos, C.A. (2015). Tumor indoleamine 2,3-dioxygenase (IDO) inhibits CD19-CAR T cells and is downregulated by lymphodepleting drugs. Blood 125, 3905–3916.

25. Moschella, F., Torelli, G.F., Valentini, M., Urbani, F., Buccione, C., Petrucci, M.T., Natalino, F., Belardelli, F., Foà, R., and Proietti, E. (2013). Cyclophosphamide induces a type I interferon-associated sterile inflammatory response signature in cancer patients' blood cells: implications for cancer chemoimmunotherapy. Clin. Cancer Res. 19, 4249–4261.

26. Schiavoni, G., Sistigu, A., Valentini, M., Mattei, F., Sestili, P., Spadaro, F., Sanchez, M., Lorenzi, S., D'Urso, M.T., Belardelli, F., et al. (2011). Cyclophosphamide synergizes with type I interferons through systemic dendritic cell reactivation and induction of immunogenic tumor apoptosis. Cancer Res. 71, 768–778.

27. Visioni, A., Kim, M., Wilfong, C., Blum, A., Powers, C., Fisher, D., Gabriel, E., and Skitzki, J. (2018). Intra-arterial Versus Intravenous Adoptive Cell Therapy in a Mouse Tumor Model. J. Immunother. 41, 313–318.

28. Innamarato, P., Kodumudi, K., Asby, S., Schachner, B., Hall, M., Mackay, A., Wiener, D., Beatty, M., Nagle, L., Creelan, B.C., et al. (2020). Reactive Myelopoiesis Triggered by Lymphodepleting Chemotherapy Limits the Efficacy of Adoptive T Cell Therapy. Mol. Ther. 28, 2252–2270.

29. Elia, A.R., Caputo, S., and Bellone, M. (2018). Immune Checkpoint-Mediated Interactions Between Cancer and Immune Cells in Prostate Adenocarcinoma and Melanoma. Front. Immunol. 9, 1786.

30. Pistillo, M.P., Carosio, R., Banelli, B., Morabito, A., Mastracci, L., Ferro, P., et al. (2019). IFN-γ upregulates membranous and soluble PD-L1 in mesothelioma cells: potential implications for the clinical response to PD-1/PD-L1 blockade. Cell. Mol. Immunol. 17, 410–411.

31. Basham, J.H., and Geiger, T.L. (2016). Opposing Effects of PD-1/PD-L1/L2 Engagement and IFN-γ/TNF-α in the Treatment of AML w/ Anti-CD33 Chimeric Antigen Receptor-Modified T Cells. Blood 128, 5891–5891.

32. Wei, J., Luo, C., Wang, Y., Guo, Y., Dai, H., Tong, C., Ti, D., Wu, Z., and Han, W. (2019). PD-1 silencing impairs the anti-tumor function of chimeric antigen receptor modified T cells by inhibiting proliferation activity. J. Immunother. Cancer 7, 209.

33. Majzner, R.G., and Mackall, C.L. (2018). Tumor Antigen Escape from CAR T-cell Therapy. Cancer Discov. 8, 1219–1226.

34. Hegde, M., Mukherjee, M., Grada, Z., Pignata, A., Landi, D., Navai, S.A., Wakefield, A., Fousek, K., Bielamowicz, K., Chow, K.K., et al. (2016). Tandem CAR T cells targeting HER2 and IL13Rα2 mitigate tumor antigen escape. J. Clin. Invest. 126, 3036–3052.

35. Zah, E., Lin, M.Y., Silva-Benedict, A., Jensen, M.C., and Chen, Y.Y. (2016). T Cells Expressing CD19/CD20 Bispecific Chimeric Antigen Receptors Prevent Antigen Escape by Malignant B Cells. Cancer Immunol. Res. 4, 498–508.

36. Asnani, M., Hayer, K.E., Naqvi, A.S., Zheng, S., Yang, S.Y., Oldridge, D., Ibrahim, F., Maragkakis, M., Gazzara, M.R., Black, K.L., et al. (2019). Retention of CD19 intron 2 contributes to CART-19 resistance in leukemias with subclonal frameshift mutations in CD19. Leukemia 34, 1202–1207.

37. De Giovanni, C., Nicoletti, G., Quaglino, E., Landuzzi, L., Palladini, A., Ianzano, M.L., Dall'Ora, M., Grosso, V., Ranieri, D., Laranga, R., et al. (2014). Vaccines against human HER2 prevent mammary carcinoma in mice transgenic for human HER2. Breast Cancer Res. 16, R10–R10.

38. Zgura, A., Galesa, L., Bratila, E., and Anghel, R. (2018). Relationship between Tumor Infiltrating Lymphocytes and Progression in Breast Cancer. Maedica (Bucur) 13, 317–320.

39. Ruella, M., and June, C.H. (2018). Predicting Dangerous Rides in CAR T Cells: Bridging the Gap between Mice and Humans. Mol. Ther. 26, 1401–1403.

40. Blat, D., Zigmond, E., Alteber, Z., Waks, T., and Eshhar, Z. (2014). Suppression of murine colitis and its associated cancer by carcinoembryonic antigen-specific regulatory T cells. Mol. Ther. 22, 1018–1028.

41. Baley, P.A., Yoshida, K., Qian, W., Sehgal, I., and Thompson, T.C. (1995). Progression to androgen insensitivity in a novel in vitro mouse model for prostate cancer. J. Steroid Biochem. Mol. Biol. *52*, 403–413.

42. Hull, G.W., Mccurdy, M.A., Nasu, Y., Bangma, C.H., Yang, G., Shimura, S., Lee, H.M., Wang, J., Albani, J., Ebara, S., et al. (2000). Prostate cancer gene therapy: comparison of adenovirus-mediated expression of interleukin 12 with interleukin 12 plus B7-1 for in situ gene therapy and gene-modified, cell-based vaccines. Clin. Cancer Res. *6*, 4101–4109.

43. Saffran, D.C., Raitano, A.B., Hubert, R.S., Witte, O.N., Reiter, R.E., and Jakobovits, A. (2001). Anti-PSCA mAbs inhibit tumor growth and metastasis formation and prolong the survival of mice bearing human prostate cancer xenografts. Proc. Natl. Acad. Sci. USA *98*, 2658–2663.

44. Kern, P., Hussey, R.E., Spoerl, R., Reinherz, E.L., and Chang, H.-C. (1999). Expression, purification, and functional analysis of murine ectodomain fragments of CD8alphaalpha and CD8alphabeta dimers. J. Biol. Chem. *274*, 27237–27243.

45. Classon, B.J., Brown, M.H., Garnett, D., Somoza, C., Barclay, A.N., Willis, A.C., and Williams, A.F. (1992). The hinge region of the CD8 alpha chain: structure, antigenicity, and utility in expression of immunoglobulin superfamily domains. Int. Immunol. *4*, 215–225.

46. Kochenderfer, J.N., Yu, Z., Frasheri, D., Restifo, N.P., and Rosenberg, S.A. (2010). Adoptive transfer of syngeneic T cells transduced with a chimeric antigen receptor that recognizes murine CD19 can eradicate lymphoma and normal B cells. Blood *116*, 3875–3886.

47. Park, A.K., Fong, Y., Kim, S.I., Yang, J., Murad, J.P., Lu, J., Jeang, B., Chang, W.C., Chen, N.G., Thomas, S.H., et al. (2020). Effective combination immunotherapy using oncolytic viruses to deliver CAR targets to solid tumors. Sci. Transl. Med. *12*, eaaz1863.

48. Kim, D., Pertea, G., Trapnell, C., Pimentel, H., Kelley, R., and Salzberg, S.L. (2013). TopHat2: accurate alignment of transcriptomes in the presence of insertions, deletions and gene fusions. Genome Biol. *14*, R36.

49. Anders, S., Pyl, P.T., and Huber, W. (2015). HTSeq–a Python framework to work with high-throughput sequencing data. Bioinformatics *31*, 166–169.

50. Hsu, F., Kent, W.J., Clawson, H., Kuhn, R.M., Diekhans, M., and Haussler, D. (2006). The UCSC Known Genes. Bioinformatics *22*, 1036–1046.

51. Mortazavi, A., Williams, B.A., McCue, K., Schaeffer, L., and Wold, B. (2008). Mapping and quantifying mammalian transcriptomes by RNA-Seq. Nat. Methods *5*, 621–628.

52. Lawrence, M., Huber, W., Pagès, H., Aboyoun, P., Carlson, M., Gentleman, R., Morgan, M.T., and Carey, V.J. (2013). Software for computing and annotating genomic ranges. PLoS Comput. Biol. *9*, e1003118.

53. Subramanian, A., Tamayo, P., Mootha, V.K., Mukherjee, S., Ebert, B.L., Gillette, M.A., Paulovich, A., Pomeroy, S.L., Golub, T.R., Lander, E.S., and Mesirov, J.P. (2005). Gene set enrichment analysis: a knowledge-based approach for interpreting genome-wide expression profiles. Proc. Natl. Acad. Sci. USA *102*, 15545–15550.

54. Liberzon, A., Birger, C., Thorvaldsdóttir, H., Ghandi, M., Mesirov, J.P., and Tamayo, P. (2015). The Molecular Signatures Database (MSigDB) hallmark gene set collection. Cell Syst. *1*, 417–425.

55. Ashburner, M., Ball, C.A., Blake, J.A., Botstein, D., Butler, H., Cherry, J.M., Davis, A.P., Dolinski, K., Dwight, S.S., Eppig, J.T., et al.; The Gene Ontology Consortium (2000). Gene ontology: tool for the unification of biology. Nat. Genet. *25*, 25–29.